Article

Improvement in diabetic retinopathy through protection against retinal apoptosis in spontaneously diabetic Torii rats mediated by ethanol extract of *Osteomeles schwerinae* C.K. Schneid.

Chan-Sik Kim[1+,5], Junghyun Kim[2,3+], Young Sook Kim[1+], Kyuhyung Jo[1], Yun Mi Lee[2], Dong Ho Jung[2], Ik Soo Lee[2], Joo Hwan Kim[4], and Jin Sook Kim[2*]

[1] Clinical Medicine Division, Korea Institute of Oriental Medicine, Daejeon 34054, Republic of Korea
[2] Herbal Medicine Research Division, Korea Institute of Oriental Medicine, Daejeon 34054, Republic of Korea
[3] Department of Oral pathology, School of Dentistry, Chonbuk National University, Jeonju 54896, Republic of Korea
[4] Department of Life Science. Gachon University, 1342, Seongnamdaero, Seongnam, Gyeonggido 13120, Republic of Korea
[5] Korean Medicine Life Science, University of Science Technology (UST), Daejeon 34113, Republic of Korea

[*]Correspondence: jskim@kiom.re.kr; +82-42-868-9465
[+]These authors contributed equally to this work.

Abstract: Retinal apoptosis plays a critical role in the progression of diabetic retinopathy (DR), a common diabetic complication. Currently, the tight control of blood glucose levels is the standard approach to prevent or delay the progression of DR. However, prevalence of DR among diabetic patients remains high. Focusing on natural nutrients or herbal medicines that can prevent or delay the onset of diabetic complications, we administered an ethanol extract of the aerial portion of *Osteomeles Schwerinae* (OSSCE), a Chinese herbal medicine, over a period of 17 weeks to spontaneously diabetic Torii (SDT) rats. OSSCE was found to ameliorate retinal apoptosis through the regulation of advanced glycation end products (AGEs) accumulation, oxidative stress, and mitochondrial function via inhibition of NF-κB activity, in turn through the downregulation of PKCδ, P47phox, and ERK1/2. We further demonstrated in 25 mM glucose-treated human retinal microvascular endothelial cells (HRMECs) that hyperoside (3-O-galactoside-quercetin), quercitrin (3-O-rhamnoside-quercetin), and 2''-O-acetylvitexin (8-C-(2''-O-acetyl-glucoside)-apigenin) were the active components of OSSCE that mediated its pharmacological action. Our results provide evidence that OSSCE is a powerful agent that may directly mediate a delay in development or disease improvement in patients of DR.

Keywords: *Osteomeles Schwerinae;* diabetic retinopathy (DR); spontaneously diabetic Torii (SDT) rat; human retinal microvascular endothelial cells (HRMECs); advanced glycation end products (AGEs); retinal apoptosis; oxidative stress; mitochondrial function; adjunctive effect; combination therapy

1. Introduction

Diabetic retinopathy (DR) is common long-term microvascular complication of diabetes and is a microcirculation disorder that accounts for the large majority of cases of visual impairment in working-class adults. DR has early non-proliferative and late proliferative stages [1]. Early changes in DR include apoptosis of peripheral blood cells, microvascular occlusion, vascular leakage and microaneurysm [2]. Retinal endothelial cells (REC) form the first barrier that senses changes in blood glucose and is therefore often the primary target of diabetic complications. The dysfunction of REC is a common basis for microvascular complications, including DR. Two hallmarks of human retinal cell loss in chronic diabetes have been reported – the loss of blood-retinal barrier integrity and direct effects on metabolism in the neural retina [3]. Diabetic metabolic influence on retinal neurons leads to an increase in apoptosis, which in turn causes breakdown of the blood-retinal barrier. Retinal neuronal cell death occurs early in diabetes, indicating that DR is an important risk factor for later development of neurodegeneration. The retinal neuron cells begin to die soon after the onset of streptozotocin (STZ)-induced diabetes in an experimental rat model. The increase in frequency of apoptosis occurred after only one month of induction, and a similar increase was noted in human retinas after six years of diabetes. The development of DR is usually irreversible, since retinal neurons cannot normally be replaced. This underlines the importance of deploying preventive measures in diabetic patients prior to the development of overt clinical symptoms [4]. The current therapy for patients with DR involves the tight control of blood glucose levels, with the aim of postponing disease onset and progression. Nevertheless, the prevalence of DR remains high [5]. To address this problem, at least in the form of adjunct treatment, we have used natural resources as nutrient or herbal medicine to develop an alternative preventive and/or therapeutic strategy against the onset and progression of retinal apoptosis.

Under conditions of chronic hyperglycaemia, glucose and other reducing sugars react non-enzymatically with proteins, leading to the formation of advanced glycation end products (AGEs). AGEs remain tightly bound to proteins and form intra- and inter- molecular crosslinks with adjacent proteins[6]. They have been implicated in diabetes-related complications. Their formation and accumulation damages cells in tissues such as the retinal vascular endothelium and kidney glomerular mesangium via binding interactions between them and the AGE receptor (RAGE) [7-9]. In patients with diabetes, AGEs are abnormally elevated and found accumulated in tissues and organs that form the sites for chronic diabetic complications [7]. In this vein, Hamme's group reported that AGEs accumulated in diabetic retinal vascular cells [10] promoted retinal apoptosis and vascular hyper-permeability [11]. Under hyperglycaemic conditions, oxidative stress is initiated by the generation of free radicals through protein glycation. An abnormal increase in reactive oxygen species (ROS) levels and/or decrease in antioxidant levels leads to cellular damage by hampering normal mitochondrial function. The damaged organelles trigger the apoptotic signalling pathway [12]. Oxidative stress-induced apoptosis follows the intrinsic mitochondrial pathway, with the disruption in balance between pro-apoptotic proteins such as B-cell lymphoma-2-associated X protein (Bax) and anti-apoptotic proteins such as B-cell lymphoma-1 (Bcl-1) proteins resulting in an excess of pro-apoptotic proteins in the cells, which reduces mitochondrial membrane potential ($\Delta\Psi M$) following the release of cytochrome c into the cytosol [13].

Osteomeles schwerinae C. K. Schneid (Chinese name: Huaxixiaoshiji) is recorded in the traditional Chinese book of botanical medicine, the Chinese Materia Medica. It is a species of deciduous, semi-

evergreen shrub of the family Rosaceae that is indigenous to Asia and Polynesia. It has been used in traditional Chinese folk medicine to treat various diseases, including dysentery, diarrhoea, sore throat, arthritis, neuralgia, and furuncles [14]. In our preliminary studies to uncover therapeutic agents responsible for the effects of plants shown to combat diabetic complications, it was discovered that an ethanol extract of the leaves and twigs of *O. schwerinae* (OSSCE) and two flavonoids, hyperoside and quercitrin, isolated from OSSCE, inhibited the activity of rat lens aldose reductase (RLAR) [15]. Specifically, a novel phytochemical compound, 5'-methoxy (1,1'-biphenyl)-3,4,3'-triol from OSSCE (referred to as K24) was confirmed to reduce the dilation of hyaloid-retinal vessels to near-normal values in 130 mM glucose-treated *flk: EGFP* transgenic zebrafish larvae [16]. The anti-angiogenic action of K24 was also demonstrated in an oxygen-induced retinopathy (OIR) mouse model [17]. We have previously reported that OSSCE reduces AGE/ RAGE binding interaction and the expression of TGF-β1 by pERK1/2, p38MAPK, and IκB phosphorylation in mouse glomerular mesangial cells under diabetic conditions [18]. We also used a peroxidase labelling kit-NH_2 to determine that another novel compound from OSSCE, 4-hydroxy-3',5'-dimethoxybiphenyl-(1,1'-biphenyl)-3-O-β-D-glucopyranoside (referred to as K19), inhibits non-enzymatic formation of AGE and cross-linking of AGE to collagen *in vitro*. Intravitreal injection of K19 into the *in vivo* model – AGE-modified rat serum albumin (AGE-RSA)-injected Sprague-Dawley (SD) rats – inhibited retinal vascular leakage by suppressing the expression of vascular endothelial growth factor (VEGF) and preventing the loss of occludin, an important tight junction protein[19]. Furthermore, it was also confirmed that OSSCE inhibits extracellular matrix accumulation and mesangial proliferation of glomeruli in spontaneously diabetic Torii (SDT) rats through inhibition of the interaction between platelet-derived growth factor-B chain (PDGF-BB) and PDGF-BB receptor (PDGFR-β) [20]. Hyperoside, isolated from *Abelmoschus manihot*, prevents glomerular podocyte apoptosis in STZ-induced diabetic nephropathy [21]. Hyperoside from *Allium victorialis* exhibits inhibitory effects on AGE formation and disrupted AGE-RAGE binding in hRAGE overexpressing mesangial cells [22].
In this study, we investigated the inhibitory effects of OSSCE on AGE accumulation and retinal cell apoptosis in SDT rats. A multi-targeted-mode of action was confirmed in human retinal microvascular endothelial cells (HRMECs) for OSSCE and its marker compounds (MCs), quercitrin, hyperoside, and 2''-O-acetylvitexin under hyperglycaemic conditions.

2. Materials and Methods

2.1 OSSCE preparation

OSSC was collected in Kunming, Yunnan Province, China, in April 2011 and identified by Professor Joo Hwan Kim (Gachon University, Korea). A voucher specimen (no. DiAB-141) was deposited in the herbarium of Korea Institute of Oriental Medicine (KIOM), Korea. For animal and cell studies, air-dried leaves and twigs (4 kg) were extracted with EtOH three times by maceration. The combined extracts were filtered and concentrated using a vacuum evaporator, leaving behind the EtOH extract [15].

2.2 HPLC chromatogram of OSSCE

The air-dried leaves and twigs of OSSC were chopped and then extracted with 99% ethanol for 24 h at room temperature under reflux and concentrated to obtain OSSCE. Hyperoside and quercitrin

were purchased from Sigma, and 2''-O-acetylvitexin was isolated from OSSCE and identified from the spectroscopic data. HPLC analysis was performed using an Agilent 1200 HPLC instrument (Agilent Technologies, USA) equipped with a binary pump, vacuum degasser, auto sampler, column compartment, and diode array detector (DAD). The column used was a Luna C_{18} (250 × 4.6 mm/5.0 μm, Phenomex, USA). The mobile phase was composed of HPLC grade methanol (A) and 0.1% acetic acid in H_2O (B) and gradually changed as follows: from 0 min to 40 min (A: 25%–45%; B: 75%–55%); from 40 min to 55 min (A: 45%–70%; B 55%–30%); from 55 min to 65 min (A: 70%–100%; B 30%–0%); from 65 min to 70 min (A 100%). Column temperature was maintained at 30ºC. Analysis was performed at a flow rate of 1.0 mL/min and monitored at UV 254 nm.

2.3 Inhibitory activity on non-enzymatic AGE formation

Bovine serum albumin (BSA; Roche Diagnostics, Basel, Swiss) in phosphate buffer containing sodium azide (s-8032, Sigma-Aldrich, St. Louis, MO, USA) was added to a 0.2 M solution of glucose and fructose. This solution was added to the OSSCE or aminoguanidine (AG; 396494; Sigma-Aldrich), a positive control. Following 14 days of incubation, AGE-specific fluorescence was analysed using a spectrofluorometer (Synergy HT; BIO-TEK, Winooski, VT, USA; 370 nm/440 nm). The IC_{50} value was calculated from the dose inhibition curve.

2.4 Inhibitory activity on AGE formation and expression of RAGE in HRMECs

Cells were grown in DMEM/F-12 with 10% foetal bovine serum in a 5% CO_2 incubator. They were treated with either OSSCE or AG dissolved in DMSO for 1 h before addition of 25 mM HG and 500 μg/mL BSA, following which they were incubated for 24 h. To obtain the protein, cells were lysed with Laemmli sample buffer (Bio-Rad) and heated at 95°C for 5 min. Protein was separated by SDS–PAGE and transferred to a PVDF membrane using a Bio-Rad semi-blotting apparatus. The membrane was incubated with antibodies specific for AGE (1:2000, Trans Genic Inc.), RAGE (1:5000, Cell signalling), and β-actin (1:3000, Cell signalling), washed, and incubated with horseradish peroxidase-linked secondary antibodies. All sample detection and analysis was performed using LAS-3000 (Fuji Photo Film).

2.5 Animal experimental design

SDT rats 10 weeks of age and age-matched SD rats were purchased from CLEA Japan (Tokyo, Japan) and OrientBio (Korea), respectively. They were acclimated, maintained in a controlled temperature room (22 ± 2ºC in 55 ± 10% relative humidity) with a 12-h light-dark cycle. They received a basal diet (5L79, PMI Nutrition International, St Louis, MO, USA) and tap water ad libitum for 14 weeks until the blood glucose levels of SDT rats reached 300 mg/dL. At 24 weeks of age, the rats were randomly divided into four groups: (1) normal SD rats (Nor, n = 10), (2) vehicle-treated SDT rats (SDT, n = 10), (3) SDT rats treated with 100 mg/kg/day of OSSCE (OSSCE-100, n = 10) and (4) SDT rats treated with 250 mg/kg/day of OSSCE (OSSCE-250; n = 10). OSSCE was dissolved in distilled water and administered once a day orally for 17 weeks. All 42-week-old rats were sacrificed. All animal

care procedures were approved by the Institutional Animal Care and Use Committee of KIOM (IACUC Approval number HH109037). Blood samples were obtained at the time of sacrifice. Blood glucose level was measured with an automated biochemistry analyser (HITACHI 917, Japan), and glycated haemoglobin was determined by a commercial kit (Unimate HbA1c, Roche Diagnostic, Mannheim, Germany) [20].

2.6 Cell culture

Human retinal microvascular endothelial cells (HRMECs) were purchased from Cell Systems (Cat. No. ACBRI 181, Kirkland, WA, USA) and used at passages 3–7. Cells were grown in CSC complete medium (CS-4ZO-500; Cell Systems) containing Bac-Off® (antibiotic). Cultures were maintained at 37°C in a humidified 95% air/5% CO_2 atmosphere [23].

2.7 Western blot analysis

Cells were treated with Laemmli sample buffer (Cat. No. 161-0737, Bio-Rad, CA, USA) and heated to 100°C for 5 min. Proteins were electrophoresed at 20 μg/lane on a denaturing SDS–polyacrylamide gel and transferred to a nitrocellulose membrane (Whatman, GmbH, Hahne str., Germany) using a Bio-Rad tank blotting apparatus (Bio-Rad, Hercules, CA, USA). Membranes were probed with 1:1000–1:2000 dilutions of primary antibodies against p47 Phox (Santa Cruz Biotechnology), ERK1/2 (Cell Signaling Technology, Danvers, MA, USA), PKC_δ (Santa Cruz Biotechnology) and β-actin (Sigma). The membrane was washed and incubated with a horseradish peroxidase-coupled goat anti-rabbit IgG (Santa Cruz Biotechnology). After washing the membranes thrice, signals were detected with a WEST-one ECL solution (Intron, Korea) using a Fujifilm LAS-3000 (LAS-3000, Fuji Photo, Tokyo, Japan). The band intensities were determined using Multi Gauge Version 3.0 software.

2.8 TUNEL staining

The rat retinal vessel was fixed with 4% paraformaldehyde. TUNEL staining was performed with a Dead End Fluorometric TUNEL kit as per the manufacturer's instructions (Promega, Madison, WI, USA).

2.9 IKK complex assay

IKK activity was evaluated using an IKK-β inhibitor screening kit (Calbiochem, CA, USA) according to the manufacturer's instructions.

2.10 Morphological observation of mitochondria

For assessment of mitochondrial morphology in living cells, mitochondria were stained with MitoTracker red (Life Technologies, USA) and phalloidin (Santa Cruz, USA) for 30 min at 37°C in a humidified chamber with 5% CO_2. Images were taken using an Olympus FV10i confocal microscope.

To observe individual mitochondria, z-stack images were acquired in series of six slices per cell ranging in thickness from 0.5 to 0.8 μm per slice.

2.11 Mitochondrial membrane potential (ΔΨm) analysis

The lipophilic cationic probe JC-1 (Abcam, USA) was employed to measure the mitochondrial membrane potential (ΔΨm) of cells according to the manufacturer's directions. Cells were incubated with 5 μg/mL JC-1 for 20 min and rinsed with JC-1 staining buffer. The fluorescence intensity of mitochondrial JC-1 monomers (green) and aggregates (red) was detected using an Olympus microscope (BX51, Olympus, Japan). In healthy cells with high mitochondrial ΔΨm, JC-1 forms complexes that emit intense red fluorescence (JC-1 aggregates). In apoptotic cells with low ΔΨm, JC-1 remains in monomeric form, and emits green fluorescence. The ratio of red to green fluorescence was calculated by analysing the digital images using Image J software (National Institutes of Health, MD, USA) and was indicative of the ΔΨm.

2.12 Intracellular ROS measurement

Measurement of intracellular ROS level was made using dihydrodichlorofluorescein diacetate (DCF-DA), in which the fluorescent probe, 2',7'-dichlorodihydrofluorescein diacetate (H_2DCF-DA; Molecular Probes Inc., Eugene, OR, USA), was converted by intracellular esterase to H_2DCF, which was oxidized by intracellular ROS to the highly fluorescent DCF. OSSCE or MCs treatment was administered for 10 min, and the cells were then stimulated with HG for 96 h. Cells were washed with HBSS buffer and incubated in the dark for 30 min in HBSS buffer containing 50 μM H_2DCF-DA. DCF fluorescence was measured using a Synergy HT spectrofluorometer (ex. 485 nm/em. 530 nm, BIO-TEK, VT, USA). The production of intracellular ROS was visualized by fluorescence microscopic imaging of cells incubated in the dark for 5 min in HBSS buffer containing 10 μM H_2DCF-DA, using an Olympus microscope (BX51, Olympus, Japan) equipped with an Olympus DP 70 camera.

2.13 Intracellular 8-OHdG measurements

Cells were washed with PBS, fixed, and permeabilized with 0.2% Triton X-100. Following three additional washes, cells were incubated with primary antibody against 8-OHdG (1:100, Abcam), washed, and incubated with the secondary antibody conjugated to Alexa Fluor 594. After removing the secondary antibody, cells were washed three times and observed under the inverted fluorescence microscope.

2.14 Immunocytochemistry

Cells were grown to 80% confluency in 4-well slides, synchronized, and exposed for 96 h to HG in the absence or presence of treatment solution (OSSCE or MCs). Cells were fixed for 15 min in 4% paraformaldehyde in PBS at 4°C and washed. For determination of NF-kB nuclear translocation, treated HRMECs were washed and fixed using 4% paraformaldehyde in PBS. Cells were then washed and treated with 10% goat serum in PBS for 30 min to block nonspecific binding. The primary NF-kB

antibody was diluted 1:1000 and incubated for 1 h. After further washing, cells were incubated with FITC for 1 h. Stained cells were sealed with mounting solution (DAKO, Glostrup, Denmark) and observed using an Olympus fluorescence microscope (BX51) equipped with an Olympus DP 70 camera.

2.15 Measurement of NADPH oxidase activity

After treatment with OSSCE or MCs, cells were washed and scraped, and then harvested with lysis buffer containing 20 mM KH_2PO_4, protease mixture inhibitor, 1 mM EGTA, 10 μg/mL aprotinin, 0.5 μg/mL PMSF at 4°C.
Following centrifugation at 10,000 g for 10 min, cell lysates were analysed immediately [24].

2.16 Statistical analysis

Image analysis was implemented using Image J software (National Institutes of Health, MD, USA) and averaged. All experiments were repeated at least three times. The data are analysed using one-way analysis of variance (ANOVA) followed by Tukey's multiple comparison test or using an unpaired Student's t-test with the Prism 6.0 software (GraphPad software, San Diego, CA, USA).

3. Results

3.1 HPLC Chromatogram of OSSCE

HPLC analysis demonstrated that hyperoside, quercitrin, and 2''-O-acetylvitexin are marker compounds for OSSCE (Fig. 1).

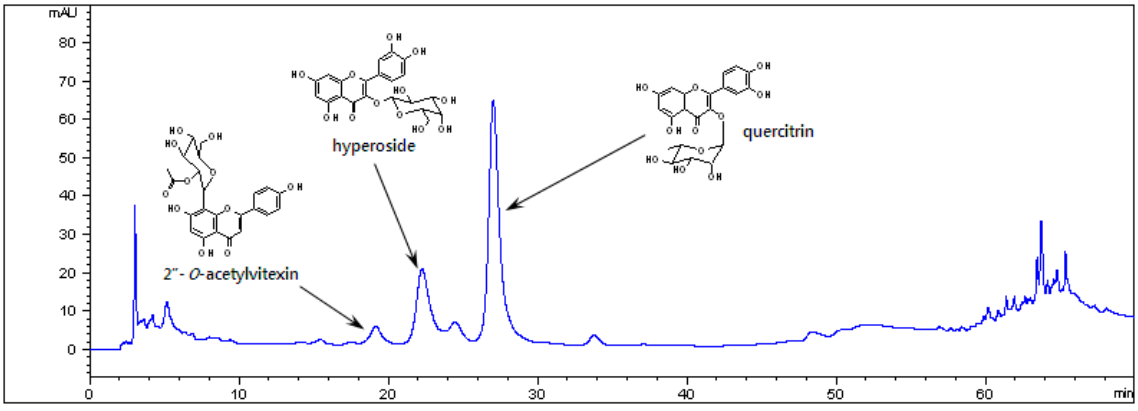

Figure 1. HPLC chromatogram of ethanol extract of the aerial part of *Osteomeles Schwerinae* (OSSCE).

3.2 OSSCE inhibits AGE formation and RAGE expression in 25 mM glucose-treated HRMECs

OSSCE inhibits the non-enzymatic formation of AGEs (IC_{50}: 16.34 ± 0.04 μg/mL) more effectively than aminoguanidine (AG), an established AGE inhibitor (IC_{50}: 72.28 ± 4.21 μg/mL) (Fig. 2a). HRMECs were treated with 10 ng/mL OSSCE or 10 nM doses of the three identified MCs, and then incubated with 25 mM glucose (HG). OSSCE- and MC-treated HRMECs showed a marked reduction

in the formation of AGEs compared with vehicle-treated HRMECs (###P < 0.001). OSSCE and quercitrin significantly reduced the expression of RAGE (##P < 0.01, #P < 0.05). RAGE expression in hyperoside- and 2''-O- acetylvitexin-treated groups exhibited a decreasing trend (Fig. 2b). Concentration of serum AGEs was prominently increased in vehicle-treated SDT rats compared with normal SD rats (**P < 0.01). OSSCE treatment (250 mg/kg/day) significantly decreased AGEs levels in SDT rats relative to vehicle-treated rats (#P < 0.05) (Fig. 2c). Whole retinal tissue from vehicle-treated SDT rats showed significant accumulation of AGEs relative to normal SD rats (**P < 0.01). High doses of OSSCE significantly reduced levels of AGEs relative to levels in vehicle-treated SDT rats (#P < 0.05) (Fig. 2d).

(a)

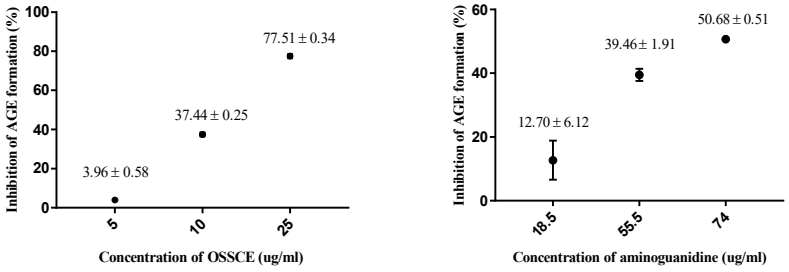

(b)

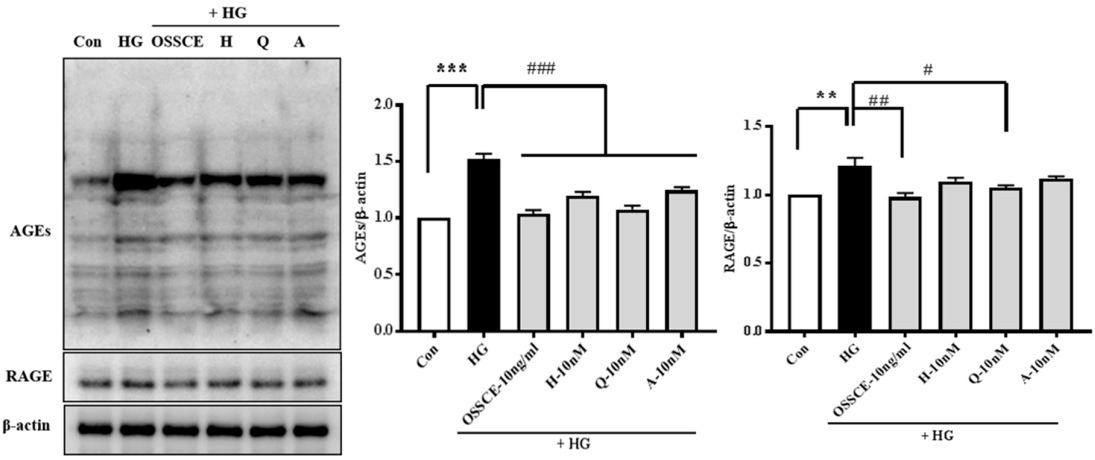

(c)

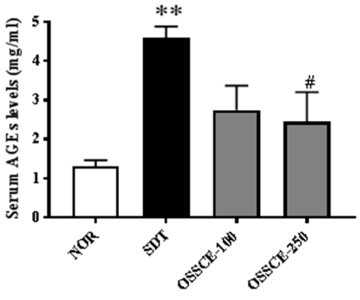

(d)

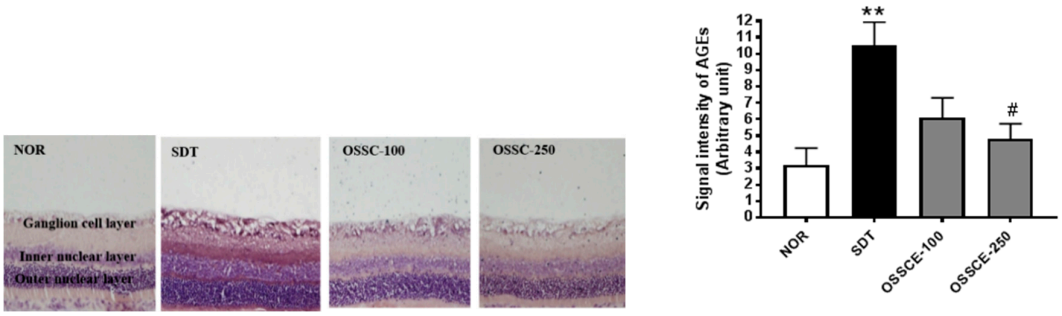

Figure 2. OSSCE inhibits non-enzymatic AGE formation, AGE formation and RAGE expression in HG-treated HRMECs. (a) Inhibitory action of OSSCE on non-enzymatic AGEs formation. Aminoguanidine (AG) was used as a positive control. OSSCE was added into the solution of BSA and 0.2 M glucose and fructose, and incubated for 14 days, AGE-specific fluorescence was analysed using a spectrofluorometer. The IC_{50} value was calculated from the dose inhibition curve. IC_{50} values of OSSCE and AG activity against non-enzymatic AGE formation are 16.34 ± 0.04 μg/mL and 72.28 ± 4.21 μg/mL, respectively (n = 3). (b) Inhibitory effect of OSSC and MCs on AGE formation and RAGE expression in HG-treated HRMECs. Con, HG, H, Q, A stand for control, 25 mM glucose, hyperoside, quercitrin, and 2''-O-acetylvitexin, respectively. HG incubation for 96 h was performed after treatment with OSSCE or MCs. Cell lysate was subjected to western blotting with monoclonal antibodies against specific AGEs, RAGE, and β actin, as described in Materials. All data are expressed as the mean ± SD (n = 3). ***$p < 0.001$, **$p < 0.01$ vs. Con.; ###$p < 0.001$, ##$p < 0.01$, #$p < 0.05$ vs. HG. AGEs level in serum (c) and whole retina (d) of SDT rats. OSSCE was administered at 100 or 250 mg/kg/day orally for 17 weeks. Serum AGEs levels were analysed by ELISA. AGEs in rat retinas were analysed by immunofluorescence staining and western blot analysis followed by densitometric quantification. **$p < 0.01$ vs. NOR; #$p < 0.05$ vs. SDT. **$p < 0.01$ vs. NOR; #$p < 0.05$ vs. SDT. Data are expressed as means ± S.D. (n = 3–5).

3.3 OSSCE inhibits apoptosis of the retinal ganglion cell layer and whole retinal vessels in SDT rats

To confirm the inhibitory effect of OSSCE on retinal damage, we investigated levels of apoptosis in SDT rat tissues. We applied the terminal deoxynucleotidyl transferase dUTP nick end labelling (TUNEL) assay in trypsin-digested retinal ganglion cells and in whole retinal vessels. The retinal trypsin digests were analysed to quantitate TUNEL-positive cells. Examination of the retinal trypsin digests of vehicle-treated SDT rats showed dramatic increases in TUNEL-positive cells in the retinal ganglia (**$p < 0.01$) and in whole retinal vessels (***$p < 0.001$) relative to that seen in normal SD rats. OSSCE-treated SDT rats exhibited a significant reduction in the number of TUNEL-positive cells in the ganglion layer (#$p < 0.05$) relative to vehicle-treated SDT rats (Fig. 3a). Levels of apoptosis in whole retinal vessels of SDT rats treated with two different dosages of OSSCE (18 ± 11%, 11 ± 9%) reduced by 67% and 78% respectively relative to the levels seen in vehicle-treated SDT rats (45 ± 15%) (##$p <$ 0.01; ###$p < 0.001$) (Fig. 3b). We investigated further the ratio between Bax and Bcl-2 and the expression of cleaved caspase-3 in the trypsin-digested whole retina of SDT rats. The ratio of Bax to Bcl-2 in vehicle-treated SDT rats was significantly increased relative to that seen in normal SD rats (**$p < 0.01$). OSSCE-treated SDT rats exhibited a significantly reduced Bax to Bcl-2 ratio when compared with vehicle-treated SDT rats, with the decrease occurring in a dose-dependent manner (#$p < 0.05$; ##$p <$ 0.01) (Fig. 3c, left panel). Expression of cleaved caspase-3 in vehicle-treated SDT rats also increased markedly (**$p < 0.01$), but was significantly decreased in 250 mg/kg OSSCE-treated SDT rats (#$p < 0.05$) (Fig. 3c, right panel).

3.4 OSSCE and MCs inhibit HG-induced intracellular ROS generation and 8-OHdG expression in HRMECs.

Peer-reviewed version available at Nutrients 2019, 11, 546; doi:10.3390/nu11030546

HRMECs were treated with 10 ng/mL OSSCE and 10 nM MCs before incubation with HG for 96 h, and assayed for intracellular ROS generation and 8-OHdG expression using fluorescence microscopy. The HG-treated group demonstrated a significant increase in ROS generation compared with the normal group (***$p < 0.001$). The OSSCE- and MCs-treated groups exhibited significantly lower ROS production relative to the HG-treated group ($^{###}p < 0.001$) (Fig. 3d). Expression of 8-OHdG by HG was also significantly increased almost ten-fold compared to that seen in the control group ($^{***}p < 0.001$). The OSSCE- and MCs-treated groups exhibited significantly reduced expression of 8-OHdG when compared with the HG-treated group ($^{###}p < 0.001$) (Fig. 3e).

(a) (b)

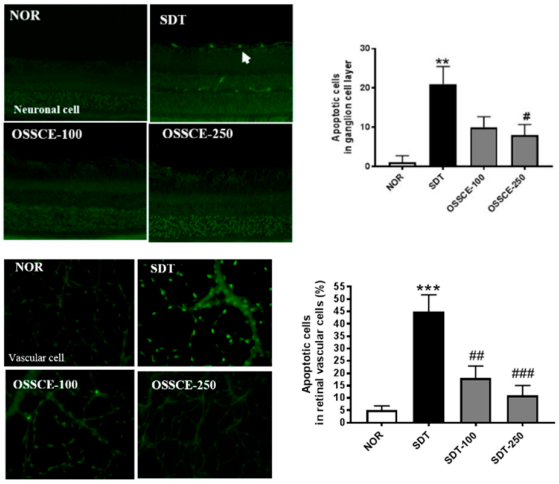

(c)

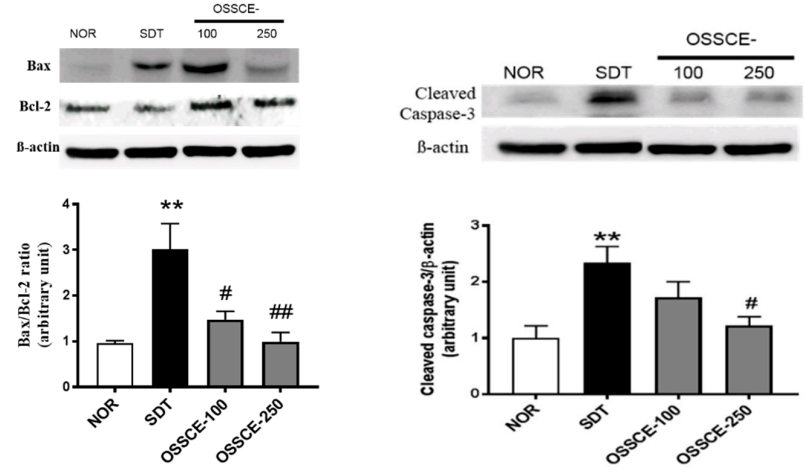

(d) (e)

Peer-reviewed version available at Nutrients 2019, 11, 546; doi:10.3390/nu11030546

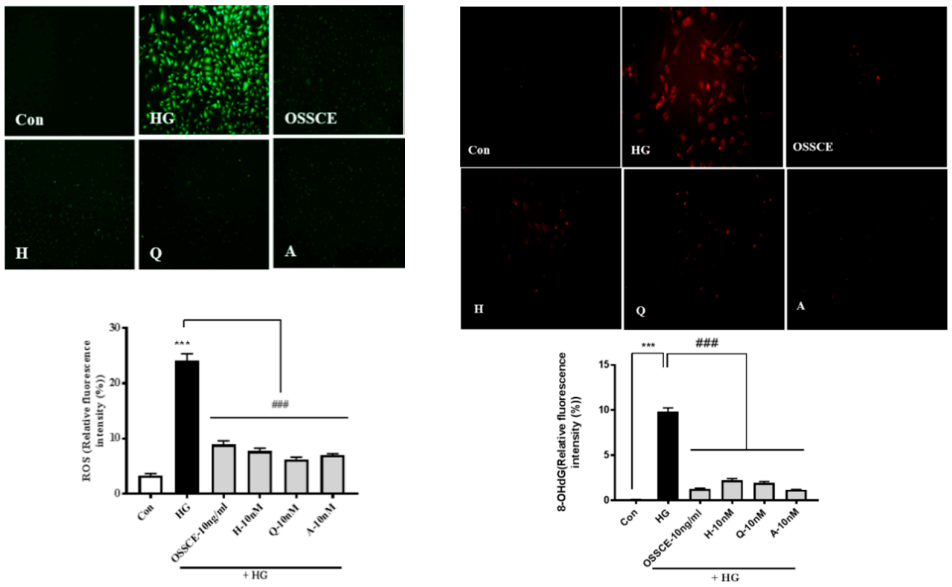

Figure 3. OSSCE inhibits retinal apoptosis in SDT rats, as well as ROS generation and 8-OHdG expression in HG-treated HRMECs. (a) OSSCE-treated groups reduce apoptosis of retinal ganglion cells and in (b) retinal microvascular vessels. Retinal sections and whole mount of retinal microvascular cells from all groups were stained with TUNEL kit, following which TUNEL-positive cells were analysed. $^{***}p < 0.001$, $^{**}p < 0.01$ vs. NOR; $^{\#}p < 0.05$, $^{\#\#}p < 0.01$, $^{\#\#\#}p < 0.001$ vs. SDT. (c) Retinal sections in all groups were stained with Bax, Bcl-2 and cleaved caspase-3 antibodies and their expression levels were measured quantitatively by western blot. The ratio of Bax to Bcl-2 and the levels of cleaved caspase-3 in SDT rat retinas increased in vehicle-treated SDT rats but were significantly suppressed by OSSCE. $^{**}p < 0.01$ vs. NOR; $^{\#}p < 0.05$, $^{\#\#}p < 0.01$ vs. SDT (n = 3–5). (d) Intracellular ROS levels were measured by the DCF-DA. The increase observed in HG-treated HRMECs was significantly reversed by treated with OSSCE or MCs. $^{***}p < 0.001$ vs. Con; $^{\#\#\#}p < 0.001$ vs. HG. Data are expressed as means ± S.D. (n = 3). (e) Cells were incubated with 8-OHdG-specific primary antibody and Alexa Fluor 594 anti-rabbit antibody. 8-OHdG expression was significantly decreased by treatment with OSSCE or MCs in HG-treated HRMECs. $^{***}p < 0.001$ vs. Con; $^{\#\#\#}p < 0.001$ vs. HG. Data are expressed as means ± S.D. (n = 3).

3.5 Protective effects of OSSCE and MCs on HG-induced mitochondrial morphology and mitochondrial membrane potential (ΔΨM) in HRMECs

Mitochondrial tubules in the HG-treated group became shorter and more fragmented compared to those from the untreated group. However, OSSCE and the MCs were found to prevent such mitochondrial damage (Fig. 4a). We evaluated the effect of OSSCE and MCs on HG-induced ΔΨM in HRMECs by detecting different fluorescence emitted by monomeric and aggregated 5, 5', 6, 6'-tetrachloro-1, 1', 3, 3'-tetramethyl benzimidazolyl carbocyanine iodide (JC-1). Depolarization of the mitochondrial membrane was evidenced by the green fluorescence emitted by HG-treated cells resulting from the presence of JC-1 in monomeric form. Untreated cells, on the other hand, emitted red fluorescence due to the aggregation of JC-1. Reduced red/green fluorescence intensity ratio can thus indicate the depolarization of mitochondria. Fig. 4b (left panel) indicates that HREMCs exposed to HG for 24 h exhibited a significant decrease in the aggregate form (red fluorescence) and an increase in the monomeric form (green fluorescence) of JC-1. However, treatment with OSSCEs and

Peer-reviewed version available at Nutrients 2019, 11, 546; doi:10.3390/nu11030546

MCs prevented the loss of aggregation and the concurrent increase in monomers. In addition, as seen in the right panel of Fig. 4b, the HG-treated group showed greater variation in ΔΨM, as inferred from the lower range of red (hyperpolarized) to green (depolarized) colour when compared with that seen in normal cells ($p^{***} < 0.001$). However, treatment with OSSCE and MCs was found to result in a 43.2%, 39.3%, 36.1%, and 48.9% increase in the red/green fluorescence ratio of JC-1 respectively, relative to that seen in HG-treated HRMECs ($^{\#\#}p < 0.01$; $^{\#}p < 0.05$; $^{\#}p < 0.05$; $^{\#\#\#}p < 0.001$).

(a)

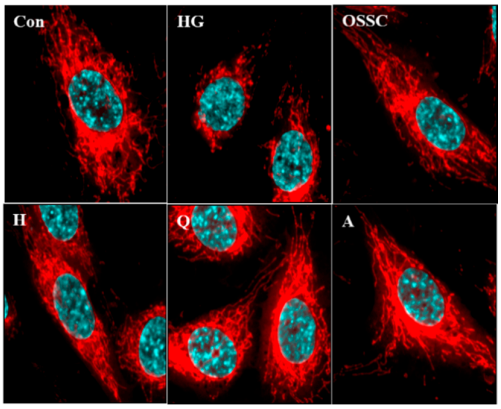

(b)

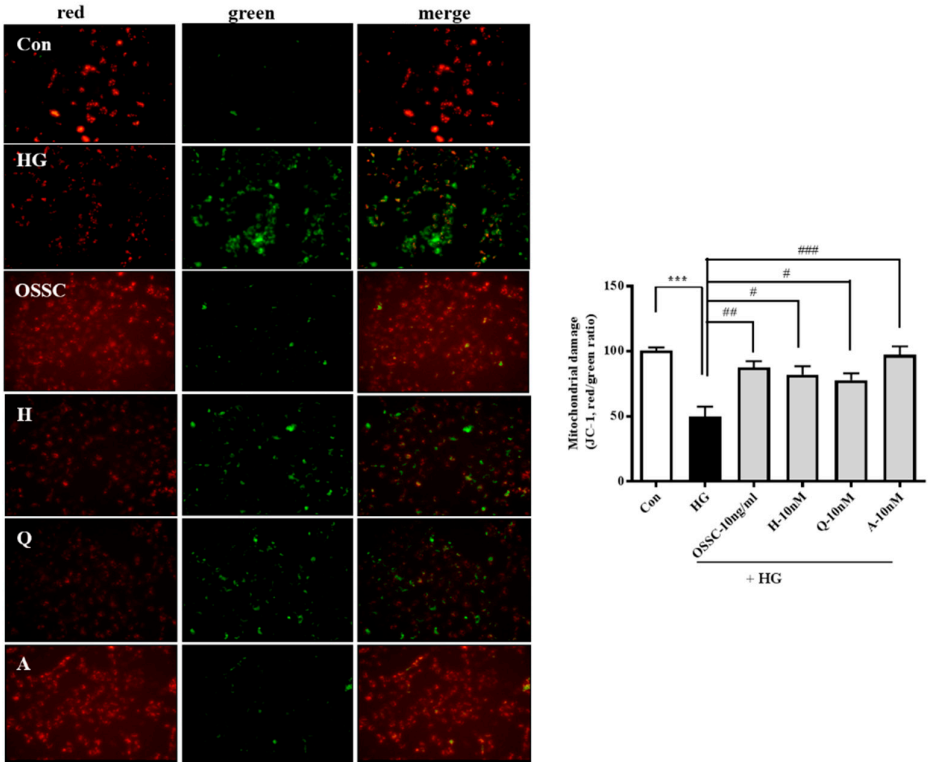

Figure 4. OSSCE and MCs inhibit the alteration of HG-induced mitochondrial morphology and mitochondrial membrane potential (MMP) activity in HRMECs. (a) OSSCE and MCs inhibit the alteration of mitochondrial shape in HG-induced HRMECs. (b, left panel) HRMECs were pre incubated with OSSCE or MCs for 24 h in the absence or presence of HG, and then the MMP was evaluated using JC-1. (b, right panel) MMP was determined using an automatic fluorescence microplate reader. The MMP (ratio of red/green) activity in the

Peer-reviewed version available at Nutrients 2019, 11, 546; doi:10.3390/nu11030546

OSSCE- and MC-treated groups showed significant increases compared with that in the HG-treated group, respectively. The red/green ratio ($\Delta\Psi m$) of HG, OSSCE, H, Q, and A was 49.75 ± 15.49, 87.61 ± 9.59, 82.01 ± 13.22, 77.87 ± 10.38, and 97.33 ± 12.96, respectively. $^{***}p < 0.001$ vs. Con; $^{\#}p < 0.05$, $^{\#\#}p < 0.01$, $^{\#\#\#}p < 0.001$ vs. HG. The data are expressed as mean ± S.D. (n = 3).

3.6. Effects of OSSCE and MCs on mitochondria-dependent apoptotic pathways in HG-treated HRMECs

Upregulation of mitochondrial Bax (Fig. 5a, left panel), cytosolic cytochrome c (Fig. 5b, right panel), and cleaved caspase-9 and -3 (Fig. 5c), and the downregulation of cytosolic Bax (Fig. 5a, lower, right) and mitochondrial cytochrome c (Fig. 5b, left panel) were observed in HG-treated HRMECs ($^{**}p < 0.01$; $^{***}p < 0.001$). OSSCE- and MCs-treated HRMECs showed significant reversal of these effects on protein expression ($^{\#}p < 0.05$; $^{\#\#}p < 0.01$; $^{\#\#\#}p < 0.001$).

(a)

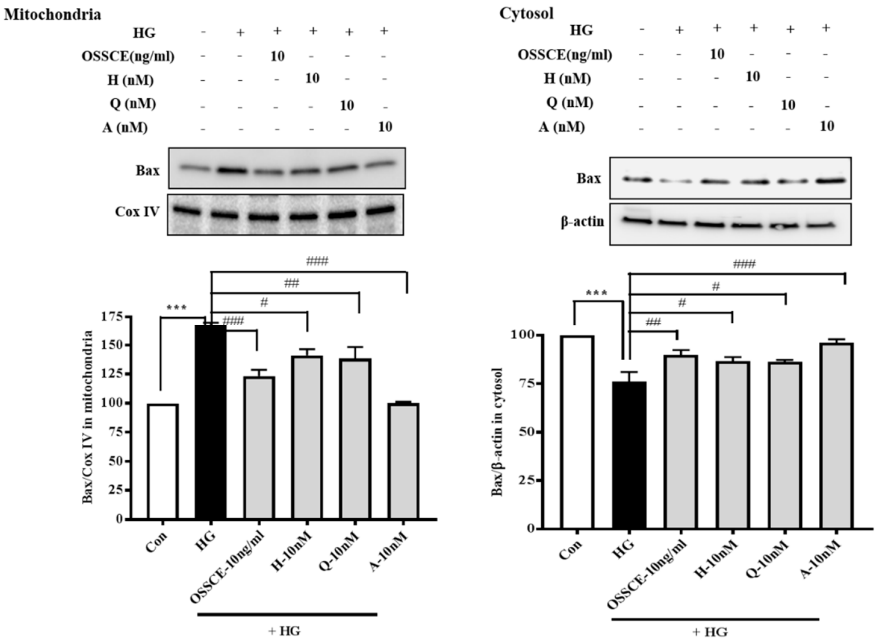

(b)

Preprints (www.preprints.org) | NOT PEER-REVIEWED | Posted: 24 January 2019 doi:10.20944/preprints201901.0245.v1

Peer-reviewed version available at Nutrients 2019, 11, 546; doi:10.3390/nu11030546

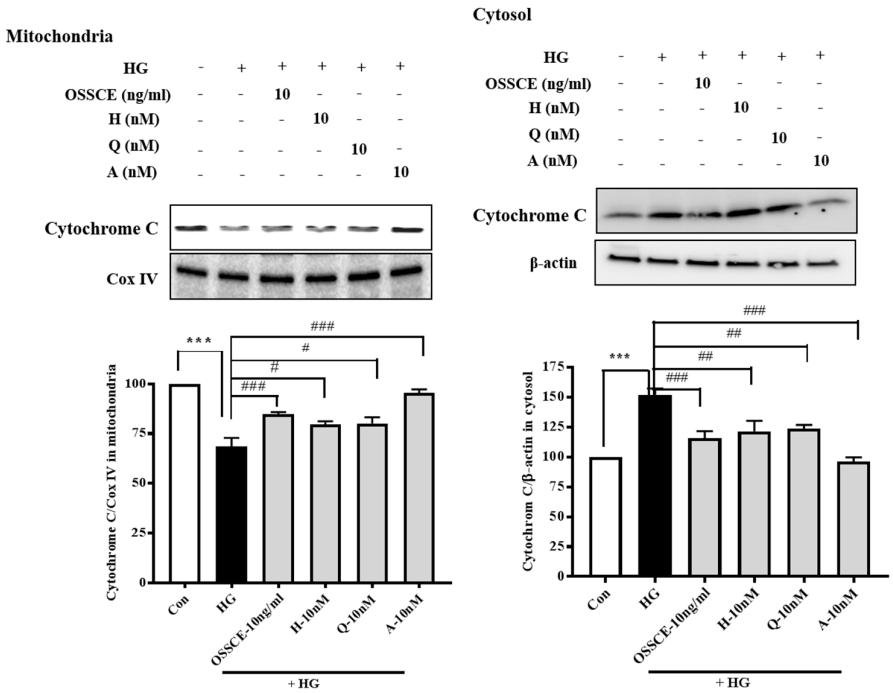

(c)

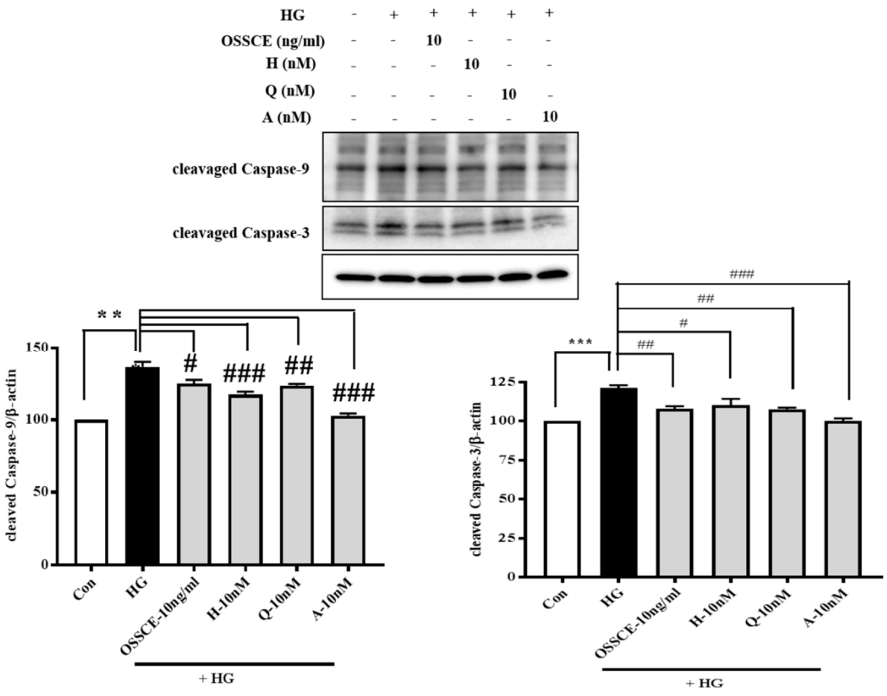

Figure 5. Effects of OSSCE and MCs on the mitochondria dependent-apoptotic pathways in HG-treated HRMECs. OSSCE and MCs restore the expression of Bax (a), cytochrome C (b) and caspase-9 and -3 (c) abnormally changed in HG-treated HRECs. $^{**}p < 0.01$, $^{***}p < 0.001$ vs. Con; $^{\#}p < 0.05$, $^{\#\#}p < 0.01$, $^{\#\#\#}p < 0.001$ vs. HG. The data are expressed as mean ± SD (n = 3).

3.7 OSSCE inhibits the activation of nuclear factor κ-B (NF-κB) in SDT rat retina and HG-treated

HRMECs

Electrophoretic mobility shift assay (EMSA) analysis of nuclear proteins revealed that OSSCE treatment at a dose of 250 mg/kg/day significantly reduced nuclear translocation and DNA-binding activity of NF-κB ($^{###}p < 0.001$), whereas vehicle-treated SDT rats resulted in increased NF-κB translocation ($^{***}p < 0.001$) relative to levels in normal SD rats (Fig. 6a).

OSSCE and MCs treatment also prevented nuclear translocation of NF-κB in HG-treated HRMECs (Fig. 6b). Visualization (Fig. 6b, left panel) and qualitative analysis of nuclear translocation (Fig. 6b, right panel) of NF-κB in HG-treated HRMECs was performed using fluorescence microscopy and Image J software respectively ($^{***}p < 0.001$). Nuclear NF-kB levels in OSSCE and MCs-treated groups of HRMECs were significantly lower than that of HG-treated group ($^{###}p < 0.001$). We checked whether OSSCE inhibited IKK activity. As shown in Fig. 6c, OSSCE treatment at doses of 50 ng/mL and 100 ng/mL dose-dependently inhibited IKK activity in HRMECs ($^{**}P < 0.01$, $^{***}P < 0.001$).

(a)

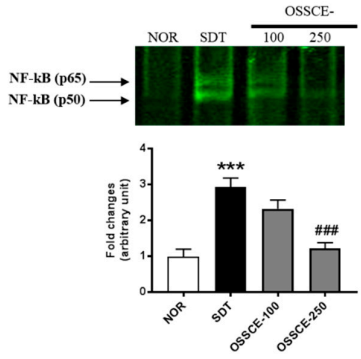

(b)

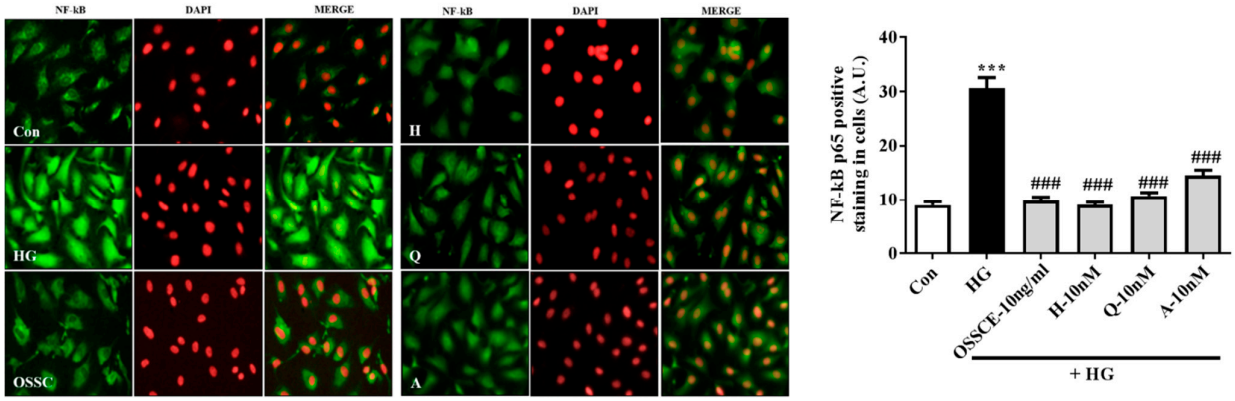

(c)

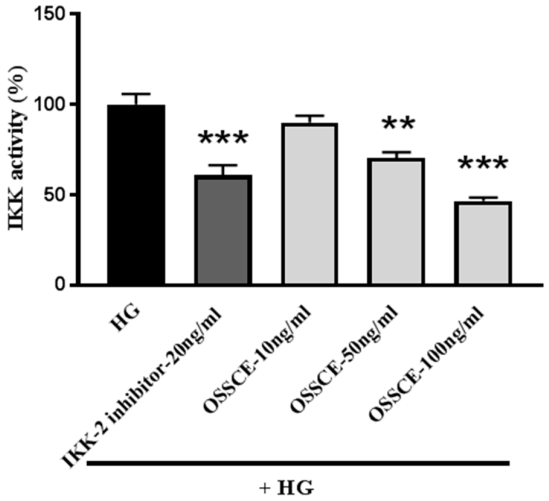

Figure 6. OSSCE inhibits the activation of NF-κB in the retina of SDT rats and in HG-treated HRMECs, and the activity of IKK-kinase. (a) Increased NF-κB activity in the retina of SDT rats was decreased by OSSCE. The NF-κB activity was measured by TUNEL staining. $^{***}p < 0.001$ vs. NOR; $^{\#\#\#}p < 0.001$ vs. SDT (n = 3–5). (b) OSSCE and MCs suppressed NF-kB translocation into the nucleus in HG-treated HRMECs (n = 4). (c) Inhibitory effect of OSSCE on the IκB kinase activity. The treatment with OSSCE at concentrations of 50 and 100 ng/mL inhibited the IκB kinase activity dose-dependently. $^{**}p < 0.01$, $^{***}p < 0.001$ vs. NOR. IKK-2 inhibitor IV (20 ng/mL) inhibited IKK activity. $^{***}p < 0.001$ vs. NOR. The data are expressed as mean ± S.D. (n = 3).

3.8. Effects of OSSCE and MCs on NADPH oxidase activity and the related signalling pathways in HG-treated HRMECs

In HG-treated cells, protein kinase C (PKC) δ was dramatically activated, although PKCα/βII and PKCζ/λ were not phosphorylated (Fig. 7a). HG-induced NADPH oxidase activity was significantly decreased by diphenyleneiodonium (DPI; NADPH oxidase inhibitor), rottlerin (PKCδ inhibitor), and GFX (PKC inhibitor), whereas Gö 6983 (PKCα/βII inhibitor) caused no such effect (Fig. 7b). We checked whether OSSCE and its MCs can regulate the activity of NADPH oxidase. NADPH oxidase in the HG-treated group was activated ($^{***}p < 0.001$) when compared with the control group. OSSCE and MCs-treated groups showed significantly reduced activity of NADPH oxidase compared with that seen in the HG-treated group ($^{\#}p < 0.05$, $^{\#\#}p < 0.01$) (Fig. 7c).

Next, we examined the inhibitory effects of OSSCE and MCs on HG-induced $p47^{phox}$, extracellular regulated kinase (ERK)-1/2, and PKCδ expression. The HG-treated group showed significantly elevated expression of PKCδ and $p47^{phox}$ compared to the control group ($^{**}p < 0.01$, $^{***}p < 0.001$). Treatment with OSSCE and MCs significantly downregulated PKCδ, and $p47^{phox}$ ($^{\#\#\#}p < 0.001$). Upregulated ERK1/2 expression caused by HG treatment was reversed by subsequent treatment with OSSCE and MCs ($^{\#\#}p < 0.01$, $^{\#}p < 0.05$) (Fig. 7d).

(a) (b)

Preprints (www.preprints.org) | NOT PEER-REVIEWED | Posted: 24 January 2019 doi:10.20944/preprints201901.0245.v1

Peer-reviewed version available at Nutrients 2019, 11, 546; doi:10.3390/nu11030546

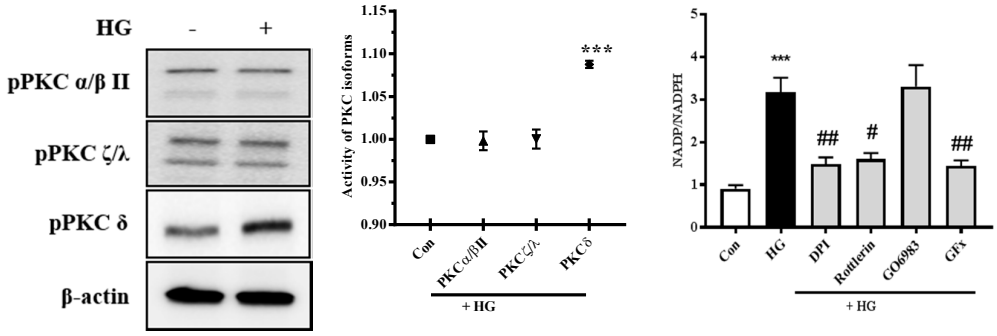

(c)

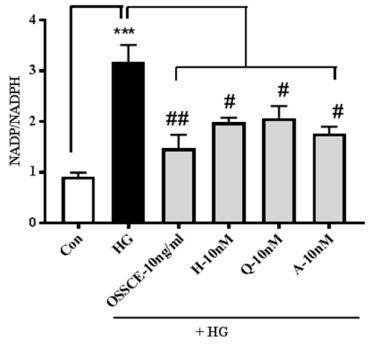

(d)

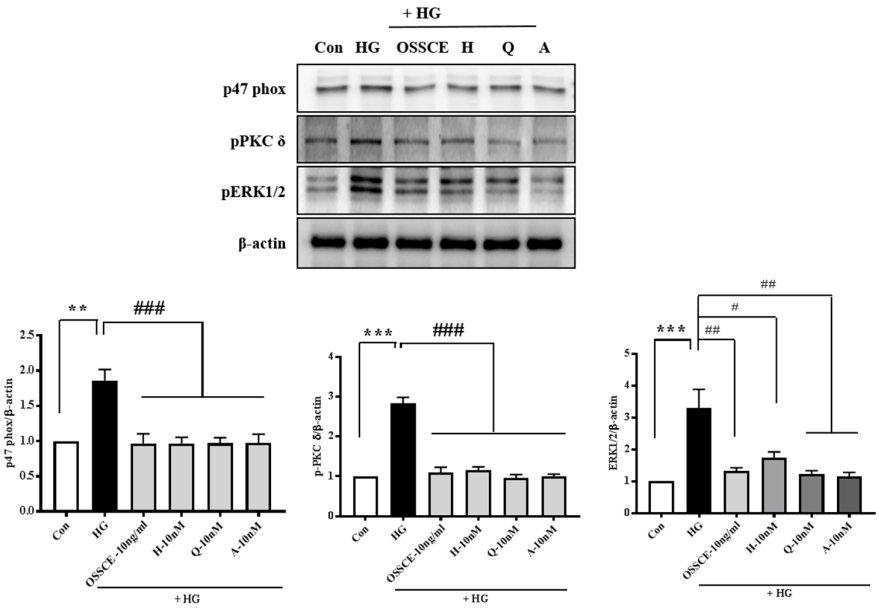

Figure 7. OSSCE and MCs inhibit the expression of HG-induced PKCδ, p47phox, and ERK1/2 in HRECs. (a) The activity of PKC isoforms was evaluated. Only PKCδ was activated under HG-treated condition. (b) The activity of NADPH oxidase was inhibited by DPI (NADPH oxidase inhibitor), rottlerin (PKCδ inhibitor), and GFx (PKC inhibitor). G06983 (PKCα/βII inhibitor) did not affect the NADPH oxidase activity. (c) OSSCE and MCs inhibit the HG-induced NADPH oxidase activity in HRMECs. The activity of NADPH oxidase was measured by the luminescence assay. $^{***}p < 0.001$ vs. Con; $^{\#}p < 0.05$, $^{\#\#}p < 0.01$ vs. HG (n = 3). (d) Elevated expression of p47phox, ERK1/2, and PKCδ due to HG was significantly restored nearly to the normal range by the treatment with OSSCE and MCs. $^{**}p < 0.01$, $^{***}p < 0.001$ vs. Con; $^{\#}p < 0.05$, $^{\#\#}p < 0.01$, $^{\#\#\#}p < 0.001$ vs. HG. All the data are expressed as mean ± SD (n = 3).

3.9. Levels of haemoglobin A1c (HbA1c) and blood glucose in SDT rats. As already reported[20], levels of HbA1c and blood glucose were significantly elevated in vehicle-treated SDT rats. However, these parameters in OSSCE-treated group showed the tendency to be decreased (Table 1).

Table 1. Levels of HbA1c and blood glucose in SDT rats

	Nor	SDT	OSSCE-100	OSSCE -250
Blood glucose (mg/dl)	144.1±21.0	419.2±21.1*	393.4±47.7	391.5±52.2
HbA1c (%)	3.49±0.07	9.13±0.37*	9.14±0.30	8.74±0.48

Nor, normal SD rat; SDT, Spontaneously diabetic Torii rat; OSSCE -100, SDT rat treated with 100 mg/kg OSSCE; OSSCE -250, SDT rat treated with 250 mg/ml OSSCE. All data were expressed as means ± SEM. *p<0.01 vs. NOR group

4. Discussion

DR is a frequent diabetic microvascular complication and one of the most common causes of legal blindness in the world. The low success of current therapeutic strategies in combating this problem points to an unmet clinical need for therapy that may slow or halt the progression of DR. It is well-known that in clinical practice, the development of diabetic complications is seen in a large number of patients even after strict control of blood glucose by oral medications, insulin therapy[25], or use of the insulin pump[26]. Clearly, there is an urgent need for the development of alternative therapeutic approaches. Matsuda's group suggested a pancreatic transplantation before the "point of no return", thereby preventing or curing diabetic complications [27]. Traditional herbal medicine, sometimes as adjunctive therapy, has been demonstrated to accrue various benefits to patients suffering from a range diseases and complications[28,29] The aim of the present study is to develop a drug candidate from herbal medicine or plant resources as a therapeutic or adjunctive approach to prevent or delay the onset of DR, including in our consideration, substances that may act through a mechanism other than the tight modulation of blood glucose levels. We investigated the potential of OSSCE against retinal apoptosis in SDT rats over a period of 17 weeks. Further, multi-targeted mode of actions for OSSCE and its MCs – hyperoside, quercitrin, and 2''-O-acetylvitexin – were also investigated in HG-treated HRMECs.

The SDT rat spontaneously develops hyperglycaemia as a result of reduced insulin secretion due to dysfunction of pancreatic islet tissues [30,31]. It has been frequently used as suitable animal model for DR. Retinal vascular leakage, vascular cell loss, and proliferative neovascularization are characteristics of SDT rats that resemble the clinical features of human DR [25,31]. Matsuda's group has reported that non-perfusion area and neovascularization in the retina were detected at 5 weeks following the onset of diabetes in SDT rats. Leakage of retinal vessels was also observed at 10 weeks post-onset of diabetes in SDT rats. Daily insulin treatment could not prevent or reverse these ocular changes. With regards to pancreatic transplantation, DR and diabetic cataract cannot be prevented or improved by performing pancreatic transplantation at or beyond 10 weeks post-onset [27].

Hyperglycaemia leads to the formation and accumulation of irreversible AGEs, which is already known to be one of the risk factors for the progression of diabetic complications such as DR. AGEs also induce apoptotic cell death of pericytes through binding interactions with RAGE [32-34]. The

IC_{50} value of OSSCE against non-enzymatic AGE formation (16.31 ± 0.04 μg/mL) was superior to that of aminoguanidine (AG; 72.28 ± 4.21 μg/mL), a well-known AGE inhibitor[35]. Further, it was confirmed that OSSCE and MCs significantly suppressed AGE formation and RAGE expression in HG-treated HRMECs (Fig. 2b). Moreover, OSSCE-treated SDT rats showed significant reduction in AGEs levels in the serum and whole retina (Fig. 2c, 2d). AGEs quantitative measurements following OSSCE treatment under HG conditions yielded coinciding results in both *in vitro* and *in vivo* contexts. Hyperglycaemia induces activation of protein kinase C (PKC) and NADPH-oxidase, which leads to the production of ROS and oxidative stress in diabetic patients. PKC and NADPH-oxidase have been suggested as potential therapeutic targets for the control of hyperglycaemia-induced oxidative stress[36]. Increased ROS production and cellular death are related. Their association is mediated by a pathological cell death pathway (apoptosis) and may be aggravated by the interaction of AGEs with RAGEs[36]. Therefore, we evaluated the effect of OSSCE on apoptosis in SDT rat retina and the associated molecular mechanisms in HG-treated HRMECs. OSSCE also exhibited an anti-apoptotic effect in the retinal ganglion cell layer (Fig. 3a arrow) and whole retinal vessels of SDT rats (Fig. 3b). We further investigated whether OSSCE could regulate apoptotic proteins in the SDT rat retina. Bax/Bcl-2 ratio and the level of caspase-3 were increased more than twofold in vehicle-treated SDT rat retinas when compared to normal SD rat retinas. These abnormal increases were significantly reversed by OSSCE treatment. Particularly, at a dosage of 250 mg/kg, they were reduced to nearly normal values (Fig. 3c). Intracellular ROS generation and increased expression of 8-OHdG in HG-treated HRMECs were prevented by the administration of OSSCE (Fig. 3c, 3d). MCs were shown to be active against oxidative stress. OSSCE reduced hyperglycaemia-induced oxidative stress, thus preventing retinal apoptosis. Oxidative stress results in alteration of mitochondrial shape and function. The change in mitochondrial shape has been linked to neurodegeneration, reduced lifespan, and cell death [37]. Dissipation of mitochondrial integrity is one of the early events leading to apoptosis [38]. Mitochondrial dysfunction is a common denominator in several chronic nervous system diseases and diabetes [39], as well as in ischemic brain injury [40].

Hyperglycaemia-induced oxidative stress increases Bax/Bcl-2 ratio, augmenting the release of cytochrome c from mitochondria to cytosol, and inducing the formation of the apoptosome. Further, it leads to the conversion of inactive procaspase 9 into active caspase 9 and procaspase 3 into caspase 3[41]. OSSCE treatment ameliorated damage to mitochondrial morphology and $\Delta\Psi M$ caused by HG in HRMECs. MCs were shown to be the active components of OSSCE responsible for this effect (Fig. 4a, 4b). OSSCE and MCs were effective in preventing the activation of the mitochondrial-dependent apoptotic pathway in HG-treated HRMECs. HG-triggered apoptosis in HRMECs occurs via the activation of caspase-9 and 3, enhancement of cytochrome C release into cytosol, and subsequent interruption of the Bax/Bcl-2 balance. These detrimental effects were prevented by OSSCE and MCs (Fig. 5a, 5b, 5c). Oxidative stress-mediated activation of NF-κB leads to the translocation of its p65 submit to the nucleus by releasing it from the inhibitory protein Iκ-Bα through Iκ-B phosphorylation [13]. Nuclear translocation of NF-kB in SDT rat retinas was significantly decreased by OSSCE treatment (250 mg/kg) (Fig. 6a). In HG-treated HRMECs, OSSCE and MCs showed marked inhibition of NF-κB translocation into the nucleus (Fig. 6b). HG-induced IκB kinase (IKK) activity was also dose-dependently decreased by OSSCE (50 ng/mL, 100 ng/mL) (Fig. 6c). That is, OSSCE was able to inhibit NF-kB translocation through the suppression of phosphorylation and degradation of IκB. OSSCE thus acts as an IKK inhibitor. NADPH oxidase is an enzyme that catalyses the production of

Peer-reviewed version available at Nutrients 2019, 11, 546; doi:10.3390/nu11030546

superoxide (O_2^-) from oxygen and NADPH. Superoxide produced by NADPH oxidase plays a critical role in diverse vascular diseases such as diabetic microvascular complications [42], stroke [43,44] and cardiovascular disease [45,46]. Activation of PKCδ and NADPH-oxidase ultimately leads to oxidative stress- and NF-kB-mediated apoptosis [36]. In the present study, among the PKC isoforms, only PKCδ was dramatically activated by HG in HRMECs (Fig. 7a). The increase in NADPH oxidase activity mediated by HG was significantly decreased by DPI, Rottlerin, and GFX, but not by Gö 6983 (Fig. 7b). These data demonstrated that PKCδ plays a crucial role in the activity of NADPH oxidase in HG-treated HRMECs. OSSCE and MCs significantly inhibited NADPH-oxidase activity by mediating a reduction in PKC_δ activity (Fig. 7c). The increased expression of PKCδ, the $p47^{phox}$ subunit of NADPH-oxidase, and ERK1/2 in HG-treated HRMECs was significantly reversed by treatment with OSSCE and MCs (Fig. 7d).

5. Conclusions

This series of experiments strongly indicated that OSSCE mediates protection against retinal apoptosis resulting from hyperglycaemia, by simultaneously modulating AGEs levels, oxidative stress-induced retinal apoptosis, and mitochondrial dysfunction through inhibition of NF-κB translocation into the nucleus via downregulation of PKCδ, $P47^{phox}$ subunit of NADPH oxidase, and ERK1/2, although OSSCE itself could not properly control the levels of blood glucose and HbA1c in SDT rats. Taken together, we can postulate that a delay and/or prevention of the development of DR might be possible, if combination of additional OSSCE and an anti-glycaemic drug such as metformin is given to patients with diabetes before the point of no return.

6. Patents

Patents related to this study were registered in Korea (no. 10-097394), Hong Kong (no. HK1170958), England, France, Swiss, Germany (no. 247483), China (no. ZL 200980160639.3), the United Arab Emirates (no.1028), and the USA (no. 8,784,911).

Author Contributions: JS Kim desined all experiments, wrote, reviewed and edited the manuscript, J kim and YS Kim designed *in vivo* and *in vitro* studies; CS kim, J Kim, KH Jo and YM Lee performed animal experiments; YS Kim and DH Jung performed *in vitro* experiments; IK Lee confirmed HPLC Chromatogram; JH Kim collected and identified OSSC.

Funding: This work was supported by Korea Institute of Oriental Medicine Grant K17270 & K18270.

Conflicts of Interest: The authors declare no competing interests.

Data Availability: All data generated or analysed during this study are included in this published article.

References

1. Fong, D.S.; Aiello, L.; Gardner, T.W.; King, G.L.; Blankenship, G.; Cavallerano, J.D.; Ferris, F.L., 3rd; Klein, R.; American Diabetes, A. Diabetic retinopathy. *Diabetes Care* **2003**, *26*, 226-229.

2. Fraser-Bell, S.; Symes, R.; Vaze, A. Hypertensive eye disease: a review. *Clin Exp Ophthalmol* **2017**, *45*, 45-53, doi:10.1111/ceo.12905.
3. Barber, A.J. A new view of diabetic retinopathy: a neurodegenerative disease of the eye. *Prog Neuropsychopharmacol Biol Psychiatry* **2003**, *27*, 283-290, doi:10.1016/S0278-5846(03)00023-X.
4. Barber, A.J.; Lieth, E.; Khin, S.A.; Antonetti, D.A.; Buchanan, A.G.; Gardner, T.W. Neural apoptosis in the retina during experimental and human diabetes. Early onset and effect of insulin. *J Clin Invest* **1998**, *102*, 783-791, doi:10.1172/JCI2425.
5. Girach, A.; Manner, D.; Porta, M. Diabetic microvascular complications: can patients at risk be identified? A review. *Int J Clin Pract* **2006**, *60*, 1471-1483, doi:10.1111/j.1742-1241.2006.01175.x.
6. Vasan, S.; Foiles, P.; Founds, H. Therapeutic potential of breakers of advanced glycation end product-protein crosslinks. *Arch Biochem Biophys* **2003**, *419*, 89-96.
7. Brownlee, M. The pathological implications of protein glycation. *Clin Invest Med* **1995**, *18*, 275-281.
8. Koga, K.; Yamagishi, S.; Okamoto, T.; Inagaki, Y.; Amano, S.; Takeuchi, M.; Makita, Z. Serum levels of glucose-derived advanced glycation end products are associated with the severity of diabetic retinopathy in type 2 diabetic patients without renal dysfunction. *Int J Clin Pharmacol Res* **2002**, *22*, 13-17.
9. Miura, J.; Yamagishi, S.; Uchigata, Y.; Takeuchi, M.; Yamamoto, H.; Makita, Z.; Iwamoto, Y. Serum levels of non-carboxymethyllysine advanced glycation endproducts are correlated to severity of microvascular complications in patients with Type 1 diabetes. *J Diabetes Complications* **2003**, *17*, 16-21.
10. Hammes, H.P.; Alt, A.; Niwa, T.; Clausen, J.T.; Bretzel, R.G.; Brownlee, M.; Schleicher, E.D. Differential accumulation of advanced glycation end products in the course of diabetic retinopathy. *Diabetologia* **1999**, *42*, 728-736, doi:10.1007/s001250051221.
11. Yamagishi, S.; Nakamura, K.; Matsui, T.; Inagaki, Y.; Takenaka, K.; Jinnouchi, Y.; Yoshida, Y.; Matsuura, T.; Narama, I.; Motomiya, Y., et al. Pigment epithelium-derived factor inhibits advanced glycation end product-induced retinal vascular hyperpermeability by blocking reactive oxygen species-mediated vascular endothelial growth factor expression. *J Biol Chem* **2006**, *281*, 20213-20220, doi:10.1074/jbc.M602110200.
12. Sinha, K.; Das, J.; Pal, P.B.; Sil, P.C. Oxidative stress: the mitochondria-dependent and mitochondria-independent pathways of apoptosis. *Arch Toxicol* **2013**, *87*, 1157-1180, doi:10.1007/s00204-013-1034-4.
13. Rashid, K.; Chowdhury, S.; Ghosh, S.; Sil, P.C. Curcumin attenuates oxidative stress induced NFkappaB mediated inflammation and endoplasmic reticulum dependent apoptosis of splenocytes in diabetes. *Biochem Pharmacol* **2017**, *143*, 140-155, doi:10.1016/j.bcp.2017.07.009.
14. Song, L.; Hu, L.; Hong, X.J.S.S.; Technology Press, S., China. Chinese materia medica. **1999**, p 166.

15. Lee, J.; Jang, D.S.; Yoo, N.H.; Lee, Y.M.; Kim, J.H.; Kim, J.S. Single-step separation of bioactive flavonol glucosides from Osteomeles schwerinae by high-speed counter-current chromatography. *J Sep Sci* **2010**, *33*, 582-586, doi:10.1002/jssc.200900693.
16. Lee, I.S.; Jung, S.H.; Lee, Y.M.; Choi, S.J.; Sun, H.; Kim, J.S. Phenolic Compounds from the Leaves and Twigs of Osteomeles schwerinae That Inhibit Rat Lens Aldose Reductase and Vessel Dilation in Zebrafish Larvae. *J Nat Prod* **2015**, *78*, 2249-2254, doi:10.1021/acs.jnatprod.5b00469.
17. Lee, Y.M.; Kim, J.; Kim, C.S.; Jo, K.; Yoo, N.H.; Sohn, E.; Kim, J.S. Anti-glycation and anti-angiogenic activities of 5'-methoxybiphenyl-3,4,3'-triol, a novel phytochemical component of Osteomeles schwerinae. *Eur J Pharmacol* **2015**, *760*, 172-178, doi:10.1016/j.ejphar.2015.04.022.
18. Kim, Y.S.; Jung, D.H.; Lee, I.S.; Pyun, B.J.; Kim, J.S. Osteomeles schwerinae extracts inhibits the binding to receptors of advanced glycation end products and TGF-beta1 expression in mesangial cells under diabetic conditions. *Phytomedicine* **2016**, *23*, 388-397, doi:10.1016/j.phymed.2016.02.005.
19. Kim, C.S.; Kim, J.; Jo, K.; Lee, Y.M.; Sohn, E.; Yoo, N.H.; Kim, J.S. OSSC1E-K19, a novel phytochemical component of Osteomeles schwerinae, prevents glycated albumin-induced retinal vascular injury in rats. *Mol Med Rep* **2015**, *12*, 7279-7284, doi:10.3892/mmr.2015.4413.
20. Sohn, E.; Kim, J.; Kim, C.S.; Jo, K.; Kim, J.S. Osteomeles schwerinae Extract Prevents Diabetes-Induced Renal Injury in Spontaneously Diabetic Torii Rats. *Evid Based Complement Alternat Med* **2018**, *2018*, 6824215, doi:10.1155/2018/6824215.
21. Zhang, Z.; Sethiel, M.S.; Shen, W.; Liao, S.; Zou, Y. Hyperoside downregulates the receptor for advanced glycation end products (RAGE) and promotes proliferation in ECV304 cells via the c-Jun N-terminal kinases (JNK) pathway following stimulation by advanced glycation end-products in vitro. *Int J Mol Sci* **2013**, *14*, 22697-22707, doi:10.3390/ijms141122697.
22. Kim, Y.S.; Jung, D.H.; Lee, I.S.; Choi, S.J.; Yu, S.Y.; Ku, S.K.; Kim, M.H.; Kim, J.S. Effects of Allium victorialis leaf extracts and its single compounds on aldose reductase, advanced glycation end products and TGF-beta1 expression in mesangial cells. *BMC Complement Altern Med* **2013**, *13*, 251, doi:10.1186/1472-6882-13-251.
23. Kim, Y.S.; Jung, S.H.; Jung, D.H.; Choi, S.J.; Lee, Y.R.; Kim, J.S. Gas6 stimulates angiogenesis of human retinal endothelial cells and of zebrafish embryos via ERK1/2 signaling. *PLoS One* **2014**, *9*, e83901, doi:10.1371/journal.pone.0083901.
24. Griendling, K.K.; Minieri, C.A.; Ollerenshaw, J.D.; Alexander, R.W. Angiotensin II stimulates NADH and NADPH oxidase activity in cultured vascular smooth muscle cells. *Circ Res* **1994**, *74*, 1141-1148.
25. Tchobroutsky, G. Relation of diabetic control to development of microvascular complications. *Diabetologia* **1978**, *15*, 143-152.
26. Tamborlane, W.V.; Puklin, J.E.; Bergman, M.; Verdonk, C.; Rudolf, M.C.; Felig, P.; Genel, M.; Sherwin, R. Long-term improvement of metabolic control with the

insulin pump does not reverse diabetic microangiopathy. *Diabetes Care* **1982**, *5 Suppl 1*, 58-64.

27. Miao, G.; Ito, T.; Uchikoshi, F.; Kamei, M.; Akamaru, Y.; Kiyomoto, T.; Komoda, H.; Nozawa, M.; Matsuda, H. Stage-dependent effect of pancreatic transplantation on diabetic ocular complications in the Spontaneously Diabetic Torii rat. *Transplantation* **2004**, *77*, 658-663.

28. Kim, J.; Byun, A.R.; Kwon, S. Effect of Yeonryeonggobon-dan (YRGBD), an herbal complex, on glycemic control in patients with Type 2 diabetes mellitus: a case series. *Complement Ther Med* **2014**, *22*, 1037-1040, doi:10.1016/j.ctim.2014.09.008.

29. Kim, J.; Moon, E.; Kwon, S. Effect of Astragalus membranaceus extract on diabetic nephropathy. *Endocrinol Diabetes Metab Case Rep* **2014**, *2014*, 140063, doi:10.1530/EDM-14-0063.

30. Sasase, T.; Ohta, T.; Ogawa, N.; Miyajima, K.; Ito, M.; Yamamoto, H.; Morinaga, H.; Matsushita, M. Preventive effects of glycaemic control on ocular complications of Spontaneously Diabetic Torii rat. *Diabetes Obes Metab* **2006**, *8*, 501-507, doi:10.1111/j.1463-1326.2006.00535.x.

31. Masuyama, T.; Komeda, K.; Hara, A.; Noda, M.; Shinohara, M.; Oikawa, T.; Kanazawa, Y.; Taniguchi, K. Chronological characterization of diabetes development in male Spontaneously Diabetic Torii rats. *Biochem Biophys Res Commun* **2004**, *314*, 870-877.

32. Denis, U.; Lecomte, M.; Paget, C.; Ruggiero, D.; Wiernsperger, N.; Lagarde, M. Advanced glycation end-products induce apoptosis of bovine retinal pericytes in culture: involvement of diacylglycerol/ceramide production and oxidative stress induction. *Free Radic Biol Med* **2002**, *33*, 236-247.

33. Yamagishi, S.; Amano, S.; Inagaki, Y.; Okamoto, T.; Koga, K.; Sasaki, N.; Yamamoto, H.; Takeuchi, M.; Makita, Z. Advanced glycation end products-induced apoptosis and overexpression of vascular endothelial growth factor in bovine retinal pericytes. *Biochem Biophys Res Commun* **2002**, *290*, 973-978, doi:10.1006/bbrc.2001.6312.

34. Lecleire-Collet, A.; Tessier, L.H.; Massin, P.; Forster, V.; Brasseur, G.; Sahel, J.A.; Picaud, S. Advanced glycation end products can induce glial reaction and neuronal degeneration in retinal explants. *Br J Ophthalmol* **2005**, *89*, 1631-1633, doi:10.1136/bjo.2005.079491.

35. Thornalley, P.J. Use of aminoguanidine (Pimagedine) to prevent the formation of advanced glycation endproducts. *Arch Biochem Biophys* **2003**, *419*, 31-40.

36. Volpe, C.M.O.; Villar-Delfino, P.H.; Dos Anjos, P.M.F.; Nogueira-Machado, J.A. Cellular death, reactive oxygen species (ROS) and diabetic complications. *Cell Death Dis* **2018**, *9*, 119, doi:10.1038/s41419-017-0135-z.

37. Campello, S.; Scorrano, L. Mitochondrial shape changes: orchestrating cell pathophysiology. *EMBO Rep* **2010**, *11*, 678-684, doi:10.1038/embor.2010.115.

38. Rasola, A.; Bernardi, P. The mitochondrial permeability transition pore and its involvement in cell death and in disease pathogenesis. *Apoptosis* **2007**, *12*, 815-833, doi:10.1007/s10495-007-0723-y.

718 39. Sharma, K.; Karl, B.; Mathew, A.V.; Gangoiti, J.A.; Wassel, C.L.; Saito, R.; Pu, M.;
719 Sharma, S.; You, Y.H.; Wang, L., et al. Metabolomics reveals signature of
720 mitochondrial dysfunction in diabetic kidney disease. *J Am Soc Nephrol* **2013**, *24*,
721 1901-1912, doi:10.1681/ASN.2013020126.
722 40. Szilagyi, G.; Simon, L.; Koska, P.; Telek, G.; Nagy, Z. Visualization of mitochondrial
723 membrane potential and reactive oxygen species via double staining. *Neurosci Lett*
724 **2006**, *399*, 206-209, doi:10.1016/j.neulet.2006.01.071.
725 41. Ko, C.H.; Shen, S.C.; Hsu, C.S.; Chen, Y.C. Mitochondrial-dependent, reactive
726 oxygen species-independent apoptosis by myricetin: roles of protein kinase C,
727 cytochrome c, and caspase cascade. *Biochem Pharmacol* **2005**, *69*, 913-927,
728 doi:10.1016/j.bcp.2004.12.005.
729 42. Al-Shabrawey, M.; Bartoli, M.; El-Remessy, A.B.; Ma, G.; Matragoon, S.; Lemtalsi,
730 T.; Caldwell, R.W.; Caldwell, R.B. Role of NADPH oxidase and Stat3 in statin-
731 mediated protection against diabetic retinopathy. *Invest Ophthalmol Vis Sci* **2008**, *49*,
732 3231-3238, doi:10.1167/iovs.08-1754.
733 43. Ostrowski, R.P.; Tang, J.; Zhang, J.H. Hyperbaric oxygen suppresses NADPH
734 oxidase in a rat subarachnoid hemorrhage model. *Stroke* **2006**, *37*, 1314-1318,
735 doi:10.1161/01.STR.0000217310.88450.c3.
736 44. Didion, S.P.; Faraci, F.M. Angiotensin II produces superoxide-mediated
737 impairment of endothelial function in cerebral arterioles. *Stroke* **2003**, *34*, 2038-2042,
738 doi:10.1161/01.STR.0000081225.46324.AA.
739 45. Qin, F.; Simeone, M.; Patel, R. Inhibition of NADPH oxidase reduces myocardial
740 oxidative stress and apoptosis and improves cardiac function in heart failure after
741 myocardial infarction. *Free Radic Biol Med* **2007**, *43*, 271-281,
742 doi:10.1016/j.freeradbiomed.2007.04.021.
743 46. Zhang, L.; Zalewski, A.; Liu, Y.; Mazurek, T.; Cowan, S.; Martin, J.L.; Hofmann,
744 S.M.; Vlassara, H.; Shi, Y. Diabetes-induced oxidative stress and low-grade
745 inflammation in porcine coronary arteries. *Circulation* **2003**, *108*, 472-478,
746 doi:10.1161/01.CIR.0000080378.96063.23.

747